Ding, Xiaofeng and Rashed, Mohamed and Bozhko, Serhiy (2017) Assessment of torque ripple minimization techniques for aircraft switched reluctance machine starter/generator. In: 4th International Symposium on More Electric Aircraft Technology (MEA 2017), 8-9 Nov 2017, Beijing, China.

ASSESSMENT OF TORQUE RIPPLE MINIMIZATION TECHNIQUES FOR AIRCRAFT SWITCHED RELUCTANCE MACHINE STARTER/GENERATOR

Xiaofeng Ding, Mohamed Rashed, Christopher Ian Hill, Serhiy Bozhko

Department of Electrical and Electronic Engineering, University of Nottingham, Nottingham, UK
Xiaofeng.Ding@nottingham.ac.uk

Keywords: Torque ripple minimization, switched reluctance machine, starter-generator, more electric aircraft.

Abstract

This paper presents an assessment of different torque ripple minimization techniques for more electric aircraft Switched Reluctance Machine (SRM) starter/generator (S/G). SRM is one of the most popular potential candidates for future aircraft S/G. SRM is a type of electric machine that features simple structure hence it is cheap to manufacture, also it is very robust. However, one of the major disadvantages of SRM is that, due to its structural nature, its highly nonlinear characteristics would result in unwanted torque ripple. In order to eliminate/minimise the torque ripple, some techniques were proposed over the last decades. In this paper, several techniques of Torque ripples minimization (TRM) are introduced and then it focuses on the assessment of two techniques suitable for the proposed 45 kW SRM as S/G, namely torque sharing function (TSF) technique and a newly proposed closed-loop torque control (CLTC) technique. An analytical modelling method is also proposed in order to apply the proposed TRM techniques. Conclusions and future works are presented at the end of this paper.

1 Introduction

One of the major aims of modern more electric aircraft (MEA) design is to reduce overall on-board weight and volume [1]. Starter/generator (S/G) system is commonly recognised as one of the feasible approaches and has been studied over the last three decades [2-6]. S/G technology is to utilize a sole machine to function as motor and generator on demand. Among the researches of S/G, the most popular candidates are permanent magnet synchronous machine (PMSM) and switched reluctance machine (SRM). The major benefits of PMSM are its high-power density and well-developed control schemes while the drawback is high cost of manufacturing. On the other hand, the SRM has drawn more interests of researches mainly because of its low cost and robustness [7] while its major drawbacks are torque ripple and acoustic noises.

This study is based on a 45 kW 6/4 SRM which has been designed and manufactured for aircraft S/G application studies [8]. The simplified cross section of the proposed SRM is shown in Fig. 1.

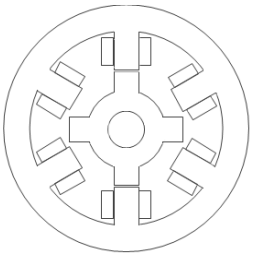

Fig. 1 Simplified cross section of proposed 6/4 SRM

The machine was designed to have the capability to operate at high speed up to 32,000 rpm in generating mode. The magnetization characteristics are shown in Fig. 2.

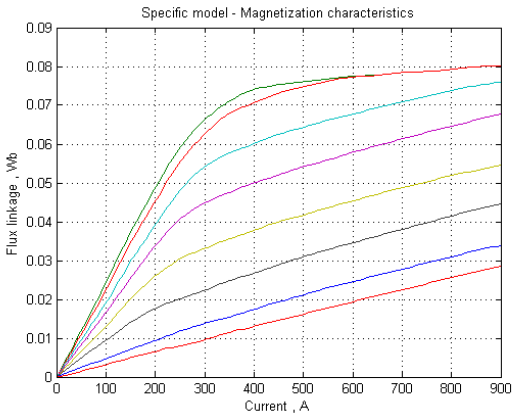

Fig. 2 Magnetization characteristics of proposed SRM

The saliences of stator and rotor in SRM introduces torque ripple to the system which will lead to vibration and acoustic noise. One of the long-time hot topics of this type of machine since its first appearance is to minimize its unwanted torque ripple. Various studies have been done regarding to this topic. Some most studied TRM techniques will be introduced in next section, followed by detailed studies and assessment of two major control based techniques.

This paper introduces several TRM techniques of SRM in literature. A new piecewise analytical modelling based on Fourier series is proposed. Torque sharing function is reviewed in details and a new direct torque control based closed-loop scheme is proposed. The assessment of these two techniques in S/G application is presented, followed by the conclusions.

2 Torque ripple minimization techniques

The major techniques of TRM can be divided into two categories. One is based on SRM structure/geometry via machine design stage while the other is based on control designs.

2.1 Motor design optimization

Torque ripple can be minimised by changing rotor structure such as rotor shifting technique introduced in [9]. By introducing the two-layer rotor structure, the overlap between rotor and stator poles is increased. The flux linkage profile of the motor is also changed hence torque curve variation is improved. In [10-11], the techniques of re-shape the stator/rotor poles are presented.

The stator/rotor pole count is usually considered as another factor which affects torque ripple. In practices, even numbers are normally selected for the counts to form a balanced multiple phase system. The rotor and stator pole counts should be reasonably close which will increase the potential average value of torque production [12]. Increase of the number of phases normally can decrease the torque ripple but also increase the cost of manufacturing. It should be noted that SRM has no self-start-up ability if the number of phases is lower than three. The proposed three-phase 6/4 SRM is a popular design choice which compromises between torque ripple, self-starting and iron losses.

2.2 Control design based torque ripple minimization

For a SRM which has been manufactured, the TRM methods will be based on control design. In this category, the major techniques which are frequently studied and improved are: direct instantaneous torque control method (DITC) [13-14] which aims to control the overall torque production directly continuously. It can be applied to hysteresis controller based scheme or pulse-width modulation (PWM) duty cycle predictive control based scheme. For torque sharing function method [15- 17], it utilises a pre-defined TSF to calculate the per phase torque demand during two phase commutations period and then generates current references with a certain shape which will apply to current control scheme. Another technique is current profiling method [18,19], which can be seen as a twist of torque sharing function. This technique also depends on generating current references for current loop control. But the algorithm of which how the current references are "profiled" is different from TSF.

In the next sections, TSF and a newly proposed closed-loop torque control will be studied and assessed in detail in the case of SRM as aircraft S/G in motoring operation.

3 TSF and closed-loop torque control based TRM techniques

In this section detailed TSF and proposed closed-loop torque control will be studied. To study the TRM techniques, the analytical modelling of studied SRM is also presented in this section.

3.1 Analytical modelling of SRM

Due to the highly non-linear characteristics of SRM, a new analytical model is proposed. It utilised the quasi-sinusoidal profile of inductance. The inductance profile can be expressed as the form of 2nd order Fourier Series functions and the functions are piecewise according to current for better accuracy. Originally a set number of measurements has been obtained in the forms of Inductance vs. excited current vs. rotor position.

The proposed inductance is presented as:

$$L(i,\theta) = a_0(i) + a_1(i)\cos(\omega_1\theta) + a_2(i)\cos(2\omega_1\theta) \quad (1)$$

when current is [0, 180A]:

$$a_n(i) = C_{0n} + C_{1n}\sin(\omega_2 i) + C_{2n}\cos(\omega_2 i) + C_{3n}\sin(2\omega_2 i) + C_{4n}\cos(2\omega_2 i), n = 0,1,2; \quad (2)$$

where $\omega_2 = \pi/(180-9)$;

By curve-fitting the measured data into the proposed 2nd order Fourier series the coefficients can be calculated as shown in Tab. 1.

Tab.1 Calculated coefficient set of low current profiles

n	C_{0n}	C_{1n}	C_{2n}	C_{3n}	C_{4n}
1	1.3878×10^{-4}	3.9072×10^{-6}	-1.9384×10^{-6}	1.9136×10^{-7}	2.5588×10^{-6}
2	1.0783×10^{-4}	3.2345×10^{-6}	-3.2287×10^{-6}	3.2653×10^{-7}	1.6264×10^{-6}
3	-7.1787×10^{-6}	-2.7000×10^{-7}	-1.9445×10^{-6}	6.0337×10^{-8}	-1.0028×10^{-6}

when current is [180, 900A]:

$$a_n(i) = D_{0n} + D_{1n}\sin(\omega_2 i) + D_{2n}\cos(\omega_2 i) + D_{3n}\sin(2\omega_2 i) + D_{4n}\cos(2\omega_2 i), n = 0,1,2; \quad (3)$$

where $\omega_2 = \pi/(900-180)$;

Same curve-fitting applied to high current situation and the coefficients are obtained as Tab. 2.

Tab.2 Calculated coefficient set of high current profiles

n	D_{0n}	D_{1n}	D_{2n}	D_{3n}	D_{4n}
1	9.9782×10^{-5}	2.3769×10^{-5}	3.2509×10^{-5}	4.2418×10^{-6}	7.0326×10^{-6}
2	6.4612×10^{-5}	3.0409×10^{-5}	2.7949×10^{-5}	7.5241×10^{-6}	5.5037×10^{-6}
3	-7.9991×10^{-6}	4.5417×10^{-6}	-6.0176×10^{-6}	2.0674×10^{-6}	-2.2849×10^{-6}

Once the analytical modelling of inductance is derived so that flux-linkage and torque profiles are obtained via the following expressions:

$$\Psi(i,\theta) = L(i,\theta)i; \tag{4}$$

$$T(i,\theta) = \partial W'(i,\theta)/\partial\theta\,|_{i=I_c} = \partial\left(\int_0^i \Psi(i,\theta)\,di\right)/\partial\theta\,|_{i=I_c}; \tag{5}$$

The analytical modelling results are shown in Fig. 3-5 in comparison of original calculated profiles from limited number of measured data.

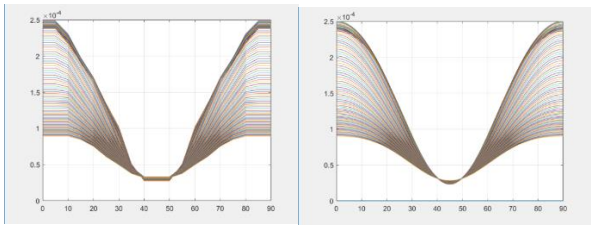

Fig. 3 Comparison of original inductance profile and analytical model

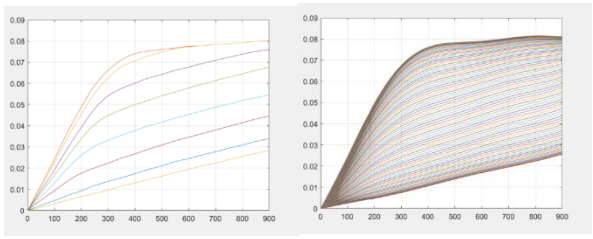

Fig. 4 Comparison of original flux-linkage profile and analytical model

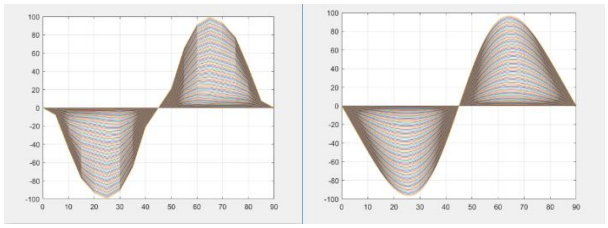

Fig. 5 Comparison of original torque profile and analytical model

An analytical modelling is a continuous model rather than lookup table which has certain intervals. It has major advantages in simulation implementation and control design purposes over the lookup table method. It saves time needed for taking numerous measurements to create the lookup table. It also can save computational memory in experimental hardware where a large quantity of data of lookup table need to be stored. Thus, in this study the analytical model is chosen rather than lookup table based model.

3.2 Torque sharing function technique

The purpose of the torque sharing function is to share the total demanded torque reference between two neighbouring phases during commutation, i.e. in the overlap zone. The TSF can be defined as linear, cubic, sinusoidal or exponential depending on the specific application. When utilising TSF, a commonly considered aspect, which as an additional objective, is to optimize the copper loss and hence enhance torque-speed capability. The typical TSF topology which combines with current hysteresis control is shown in Fig. 6.

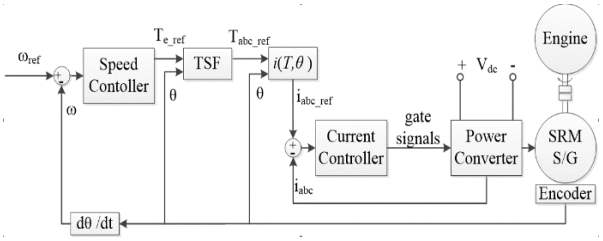

Fig. 6 Proposed TSF based S/G topology

Within this research, a sinusoidal TSF will be utilised within the control strategy for a S/G application. The expressions for the TSF can be represented by the following expressions:

$$TSF(\theta) = \begin{cases} 0, & (0 \le \theta < \theta_{on}) \\ f_{rise}(\theta), & (\theta_{on} \le \theta < \theta_{on} + \theta_{ov}) \\ T_e, & (\theta_{on} + \theta_{ov} \le \theta < \theta_{off}) \\ f_{drop}(\theta), & (\theta_{off} \le \theta < \theta_{off} + \theta_{ov}) \\ 0, & (\theta_{off} + \theta_{ov} \le \theta < \theta_p) \end{cases} \tag{6}$$

$$f_{rise}(\theta) = \frac{T_e}{2} - \frac{T_e}{2} cos\frac{\pi}{\theta_{ov}}(\theta - \theta_{on}) \tag{7}$$

$$f_{drop}(\theta) = \frac{T_e}{2} + \frac{T_e}{2} cos\frac{\pi}{\theta_{ov}}(\theta - \theta_{off}) \tag{8}$$

where θ_{on} is the turn on angle, θ_{off} is the turn off angle, θ_{ov} is the overlap angle, θ_p is the angular displacement between neighbouring phases and T_e is the total torque produced by SRM. The angles should be designed according to SRM characteristics to achieve best performance.

A typical waveform of a sinusoidal TSF is shown in Fig. 7.

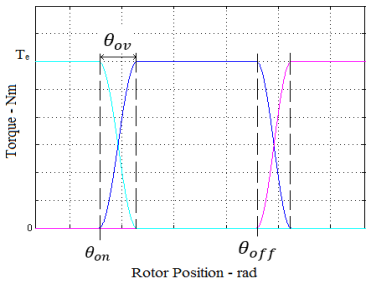

Fig. 7 Typical sinusoidal TSF waveform

The figure above shows that, during the overlap zone, the per phase torque demand has been derived according to the TSF. The total add-up torque should always equal to reference torque. The per phase reference torque is then used to calculate the per phase reference current according to its rotor position. The current references are sent to current controller to generate gate signals of power converter, thus to control the total torque production from the SRM.

Ideally, the torque production from SRM should be torque ripple-free with the aid of TSF. Fig. 8 shows a result of starting-up of the proposed SRM, with a reference torque set as 40 Nm.

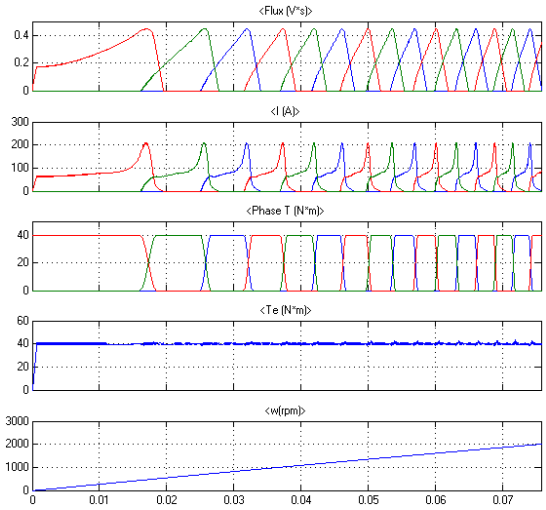

Fig. 8 Ideal torque production of SRM with TSF

3.3 Newly proposed closed-loop torque control based TRM technique

A direct torque control based closed-loop is proposed which is shown in Fig. 9. In this control scheme, the control of torque is based on a closed-loop topology where the torque error between reference torque and estimated real torque will be fed to a functional sub-block named “commutation calculator”. The inputs of the sub-block are error torque and current measurements. Inside the sub-block, it utilises error torque to determine the conduction angle of per phase current, hence switching status. The regulated current reference which required for current hysteresis controller is self-adjusted by a function according to machine speed and torque reference. The output of the sub-block is current reference for per phase which will used for current hysteresis control. Basically, the commutation calculator enables machine to work in 1st and 4th quadrants, namely forward motoring and reverse braking respectively, according to the sign of error torque. The major advantage of this topology is that when the negative error torque appears, SRM switched to reverse braking operation which will result negative per phase torque. This will force a faster rate of change of total torque production compared to 1st quadrant only topology.

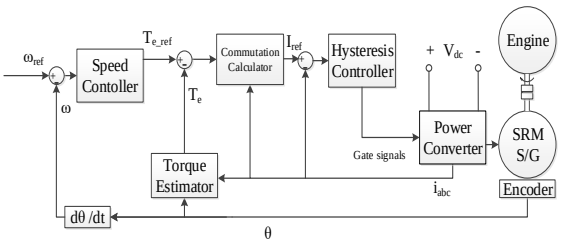

Fig. 9 The proposed closed-loop torque control scheme

For example, if the torque error is positive which means the system needs more torque production where motoring conduction angles are applied. Note that the regulated current reference of hysteresis control must make sure the SRM can produce enough torque to follow reference torque. As the real torque increases greater than reference torque which means that the torque error is negative, the conduction angles will be recalculated so that the SRM is working in reverse braking region. The advantage of carrying out this 4th quadrant operation is that the negative instantaneous per phase torque production will lead to fast drop of total torque. Once the torque drops the status of operation will change back to motoring again and repeat the process.

4 Assessment of TSF and closed-loop torque control of SRM in aircraft S/G system

In this section, these two techniques will be applied to the motoring operation of the studied 45kW 6/4 SRM. With the practical limitation considered, the evaluations are carried out for TSF in low to medium speed ranges which is 0-8000 rpms and for the proposed CLTC in higher speeds, followed by the results of assessment.

The machine is designed as 45 kW power rating, the operational characteristics are shown in Fig. 10. SRM provides constant torque of 53.7 Nm in 0-8000 rpm, then it runs in constant power region up to 16000 rpm. After engine is fully fired-up and accelerate the SRM, it will be operating in generating mode from 19200 rpm up to 32000 rpm.

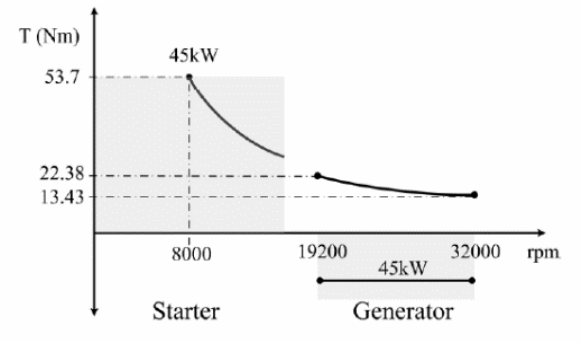

Fig. 10 Designed torque characteristics of proposed S/G

4.1 Practical limitation of power converter

In the control schemes presented in this paper, the traditional asymmetric bridge converter was designed and has the ability to take the power rating demand. However, there is an unavoidable limitation of the practical power converter implementation which is the switching frequency of gate drivers. In this case, the power converter has the maximum switching frequency of 20 kHz.

In conventional current hysteresis control where a constant regulated current reference applied for a certain average torque. To limit the switching frequency, the hysteresis band must be selected wisely for each operational condition. In low speed motoring where the SRM requires to output constant torque in S/G application. In the SRM system the voltage equation is presented as:

$$V = IR + L\frac{dI}{dt} + I\frac{dL}{d\theta}\omega \tag{9}$$

Consider the maximum switching frequency would happen when the rotor is near unaligned and moving towards aligned position, where the worst case would be the iron losses and back-emf are both neglected, hence:

$$V = L_U\frac{dI}{dt} \tag{10}$$

In this specific SRM, the inductance at unaligned position is L_U=26.6 µH. To meet the maximum switching frequency is not greater than 20 kHz, of which the period is 50 µs. Assume half of the cycle is for current to increase (in real system it will be less, thus there has been a margin), dt = 25 µs. From equation (10) it can be noted that the switching frequency can be lowered if the DC link voltage reduces. In other words, one of the solution to reduce switching frequency is to reduce DC link voltage. However, the DC link voltage is fixed as 270V for this studied case of aircraft electrical system, the overall "safe" hysteresis band then can be calculated:

$$H_{band} = dI = \frac{V}{L_U}dt = 254\ A \tag{11}$$

Note that this hysteresis band is the maximum value where it guarantees the power converter not to exceed max switching frequency of 20 kHz which means the band is not optimal. In practical, the hysteresis band should be selected to compromise between the torque ripple and power efficiency. As the limitation of switching frequency has been considered, a very wide hysteresis band must apply to this current hysteresis control in S/G application.

4.2 Assessment of TSF based technique

The evaluation criteria are selected as percentage peak-peak error and form factor K_f. As RMS value reflects the variation in the function's distance from the average, and is disproportionately impacted by large deviations from the unrectified average value, the from factor K_f which equals the RMS value divided by average can be used to evaluate the waveform distortion. e.g. when K_f is closer to 1, the waveform has less variation/distortion from average value.

A conventional hysteresis current chopping control (CCC) system in where the torque is not minimised or optimised is provided to have side-to-side comparison with TSF also with the later proposed closed-loop torque control. It has a fixed turn on angle of 40° and turn off angle 80° to make sure the CCC operates in motoring mode. By adjusting the regulated current reference, the generated average torque can be equal to the average torque produced from TSF.

In literature, most of the TSF case studies are based on a very small-scale of torque reference. That means the per phase torque production of the SRM always can provide the demand from the reference. However, the situation is very in S/G system where the high torque is demanded at lower speeds and maximum switching frequency is limited by power converter. This assessment will find out if TSF is suitable for S/G system in high torque demand at lower speeds.

In this sinusoidal TSF control scheme, the overall safe hysteresis band of 254A is applied to hysteresis controller to make sure switching frequency is no more than 20 kHz. The simulation results are shown in Fig. 11 – 14 for different scenarios of steady state motoring mode. It should be noted that all cases meet the criterion that switching frequency is not above 20 kHz. In simulation in Fig. 13, different hysteresis bands have been tested by trial and error to explore the effects of hysteresis band to the max switching frequency. When the hysteresis band is 200 A for CCC and 140 A for TSF, the max switching frequency of power converter close to 20 kHz limit.

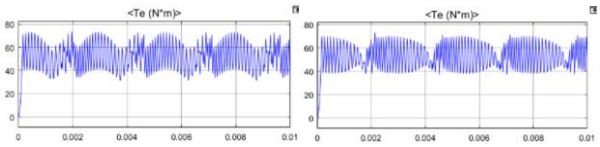

Fig. 11 Torque production by CCC and TSF at 2000 rpm, with average torque of 52.5 Nm, hysteresis band 254 A

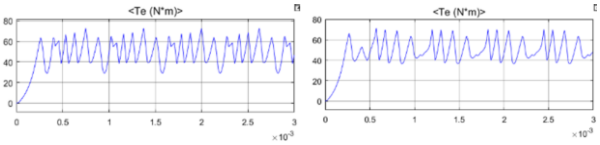

Fig. 12 Torque production by CCC and TSF at 8000 rpm, with average torque of 50.5 Nm, hysteresis band 254 A

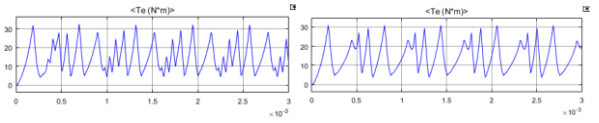

Fig. 13 Torque production by CCC and TSF at 8000 rpm, with average torque of 15 Nm, hysteresis band 254 A

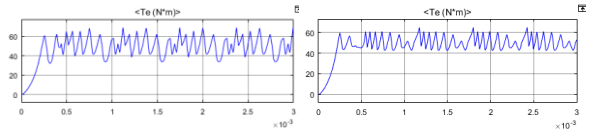

Fig. 14 Torque production by TSF and CCC at 8000 rpm, with average torque of 50.5 Nm, TSF hysteresis band 140 A, CCC hysteresis band 200 A

Tab. 3 Evaluation results of CCC and TSF

Speed (rpm)	Average Torque (Nm)	Current Chopping Control			Torque Sharing Function		
		Peak-Peak %	RMS Torque (Nm)	Form Factor K_f	Peak-Peak %	RMS Torque (Nm)	Form Factor K_f
2000	52.5	81%	53.49	1.0189	65%	53.26	1.0145
8000	50.5	85.6%	51.60	1.0218	66.7%	51.30	1.0158
8000	15.0	184.5%	16.56	1.1040	180.6%	16.53	1.1020
8000	50.5	70.3%	51.33	1.0164	44.2%	50.82	1.0063

From the results above, according to the criteria of percentage peak-peak error and form factor K_f, it shows in all cases TSF does reduce torque ripple compared to CCC. In Fig. 11 and Fig. 12 same hysteresis bands applied to both systems. As the speed increases, torque sharing function performs roughly the same while CCC does little worse than lower speed case. Comparing Fig. 13 to Fig. 12, a reduced torque demand has applied. However due to unchanged hysteresis band, the performances of both TSF and CCC go down dramatically. It is also noted that the switching frequencies in Fig. 13 are much lower than Fig. 12. Comparing Fig. 14 and Fig. 12, different hysteresis bands are applied to TSF and CCC to make sure the switching frequency is close to 20 kHz. The improvements by TSF on torque ripple reduction have been proven both visually and numerically.

The assessment of TSF in SRM based S/G system conclude that TSF is a good TRM technique which is especially beneficial to reducing the ripple caused by commutations (overlap zones). However, in this specific system, the maximum switching frequency limitation has caused very large scale of torque ripple which has much higher frequency than commutation torque ripple. If the hysteresis band is fixed for a system, because TSF has no ability to deal with the torque ripple caused by hysteresis band, the advantage of applying TSF is not too obvious in terms to TRM. The only way to improve TSF performance in this case is to change the hysteresis band to limit the ripple. Because TSF reshapes currents thus the switching sequences, the impact on the system is that the TSF would lower the switching frequency compared to CCC, so that the margin of adjusting hysteresis band is larger if one decides to apply variable hysteresis band in their control schemes.

There are cases where the per phase torque references calculated by TSF would exceed the SRM's ability. e.g. at certain rotor position such near machine pole where in general can only produce small scale of torque, the demand torque can cause an unrealistically high current reference to follow reference torque. This can be improved by machine design, especially pole shape designs. It is worth paying attend to this as one of the machine design factors if a SRM is desired to be adaptive with TSF.

4.3 Assessment of closed-loop torque control

The proposed CLTC is designed for higher speeds such as 8000 rpm – 16000 rpm in motoring mode. As the machine speed goes higher than 8000 rpm it enters constant power region, the torque reference should be changed correspondingly. The simulation results for different speeds are presented in Fig. 15-17. The regulated current of direct torque control scheme is chosen according to torque demand and the hysteresis bands in for CCC is set as variable band to make sure the max switching frequency is close to but no more than 20k Hz in different speeds. The hysteresis band for CLTC is set as 254A as it is not the main factor which determines the switching frequency in this scheme.

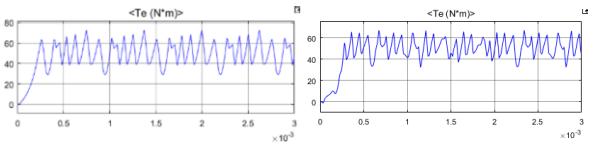

Fig. 15 CCC and CLTC at 8000 rpm, with average torque of 50.5 Nm

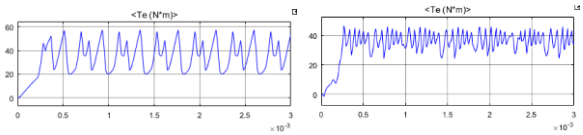

Fig. 16 CCC and CLTC at 12000 rpm, with average torque of 35.8 Nm

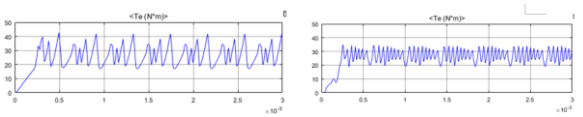

Fig. 17 CCC and CLTC at 16000 rpm, with average torque of 26.8 Nm

Tab. 4 Evaluation results CCC and CLTC

Speed (rpm)	Average Torque (Nm)	Current Chopping Control			Closed-loop Torque Control		
		Peak-Peak %	RMS Torque (Nm)	Form Factor K_f	Peak-Peak %	RMS Torque (Nm)	Form Factor K_f
8000	50.5	85.6%	51.60	1.0218	67.6%	51.20	1.0139
12000	35.8	104.7%	37.45	1.0461	59.9%	36.17	1.0103
16000	26.8	93.4%	27.53	1.0280	57.1%	27.03	1.0093

The simulation results indicate that proposed CLTC has advantages both in percentage peak-peak error and form factor in all speed cases within this constant region. In CCC, it should be noticed from the results in Tab. 4 that when the speed increases, higher back-emf leads to slower switchings and slower rate of change of phase current. It can be seen that if speed continues increasing higher than 16000 rpm, eventually CCC is no longer able to control average torque production and angle position control (APC) should be applied for higher speeds for this application.

On the other hand, because the regulated current reference which is set to vary corresponding to torque reference. It automatically fixes the switching frequency and does not allow it to go too far from the limit. Thus, the efficiency of TRM is always better than conventional CCC, it's even getting better as the speed increases unlike the CCC. This is all done by proper design of commutation calculator. It is the most crucial and difficult part of this TRM technique. Finally, the hysteresis band is another potential variable to limit the switching frequency in this topology if necessary.

5 Conclusion

In this paper, several TRM techniques of SRM were introduced. A new piecewise analytical model of SRM was proposed, followed by detailed studies of two TRM techniques – TSF and proposed closed-loop torque control. Simulations in the context of aircraft S/G system were done via Matlab/Simulink to assess the performances of the techniques. In conclusion, TSF is suitable for minimization of torque ripple which caused by phase commutations. It has limited improvements when dealing with higher frequency torque ripples which caused by hysteresis controller. The newly proposed closed-loop torque control for higher speed performs much better compared to CCC in terms of reducing torque ripple. The dynamic regulated current reference makes sure the system has optimized switching frequency.

Furthermore, the variable hysteresis band is a potential solution to compromise between torque ripple and switching frequency. It is worth studying and establishing an algorithm where hysteresis band is a function of machine speed, switching frequency limit of power converter and torque reference in future TRM studies.

6 References

[1] A. N. Reshetnikov and A. S. Khlebnikov, "Modeling of integrated starter-generator in generator mode," 2014 15th International Conference of Young Specialists on Micro/Nanotechnologies and Electron Devices (EDM), Novosibirsk, 2014, pp. 453-455.

[2] S. R. MacMinn and W. D. Jones, "A very high speed switched-reluctance starter-generator for aircraft engine applications," Proceedings of the IEEE National Aerospace and Electronics Conference, Dayton, OH, 1989, pp. 1758-1764 vol.4.

[3] S. R. MacMinn and J. W. Sember, "Control of a switched-reluctance aircraft engine starter-generator over a very wide speed range," Proceedings of the 24th Intersociety Energy Conversion Engineering Conference, Washington, DC, 1989, pp. 631-638 vol.1.

[4] C. A. Ferreira, S. R. Jones, W. S. Heglund and W. D. Jones, "Detailed design of a 30-kW switched reluctance starter/generator system for a gas turbine engine application," in IEEE Transactions on Industry Applications, vol. 31, no. 3, pp. 553-561, May/Jun 1995.

[5] M. E. Elbuluk and M. D. Kankam, "Potential starter/generator technology for future aerospace application," in IEEE Aerospace and Electronic Systems Magazine, vol. 11, no. 10, pp. 17-24, Oct. 1996.

[6] S. S. Yeoh, F. Gao, S. Bozhko and G. Asher, "Control design for PMM-based starter generator system for More Electric Aircraft," 2014 16th European Conference on Power Electronics and Applications, Lappeenranta, 2014, pp. 1-10.

[7] B. Fahimi, A. Emadi and R. B. Sepe, "A switched reluctance machine-based starter/alternator for more electric cars," in IEEE Transactions on Energy Conversion, vol. 19, no. 1, pp. 116-124, March 2004.

[8] Borg Bartolo, J. and Gerada, C., "Design and Modeling of a 45kW, Switched Reluctance Starter-Generator for a Regional Jet Application," SAE Technical Paper, 2014-01-2158, 2014

[9] M. Rafiee, A. Siadatan and E. Afjei, "Improving the Torque Ripple in SRMs Utilizing RST ", International Symposium on Power Electronics, Electrical Drives, Automation and Motion, pp.517-521, 2012.

[10] Y. K. Choi, H. S. Yoon and C. S. Koh, "Pole-Shape Optimization of a Switched-Reluctance Motor for Torque Ripple Reduction," in IEEE Transactions on Magnetics, vol. 43, no. 4, pp. 1797-1800, April 2007.

[11] K Sheth, K.R Rajagopal “Torque profiles of switched reluctance motor having special pole face shapes and Asymmetric stator poles” IEEE transactions on magnetics, vol. 40, no. 4, July 2004.

[12] R. Vandana, S. Nikam and B. G. Fernandes, "Criteria for design of high performance switched reluctance motor," Electrical Machines (ICEM), 2012 XXth International Conference on, Marseille, 2012, pp. 129-135.

[13] S. K. Singh and R. K. Tripathi, "Minimization of torque ripples in SRM drive using DITC for electrical vehicle application," Engineering and Systems (SCES), 2013 Students Conference on, Allahabad, 2013, pp. 1-5.

[14] C. R. Neuhaus, N. H. Fuengwarodsakul and R. W. De Doncker, "Predictive PWM-based direct instantaneous torque control of switched reluctance drives," 2006 37th IEEE Power Electronics Specialists Conference, Jeju, 2006, pp. 1-7.

[15] J. Ye, B. Bilgin and A. Emadi, "An Offline Torque Sharing Function for Torque Ripple Reduction in Switched Reluctance Motor Drives," in IEEE Transactions on Energy Conversion, vol. 30, no. 2, pp. 726-735, June 2015.

[16] S. Kurian and Nisha G. K., "Torque ripple minimization of SRM using torque sharing function and hysteresis current controller," 2015 International Conference on Control Communication & Computing India (ICCC), Trivandrum, 2015, pp. 149-154.

[17] V. P. Vujičić, "Minimization of Torque Ripple and Copper Losses in Switched Reluctance Drive," in IEEE Transactions on Power Electronics, vol. 27, no. 1, pp. 388-399, Jan. 2012.

[18] R. Mikail, I. Husain, M. S. Islam, Y. Sozer and T. Sebastian, "Four-Quadrant Torque Ripple Minimization of Switched Reluctance Machine Through Current Profiling with Mitigation of Rotor Eccentricity Problem and Sensor Errors," in IEEE Transactions on Industry Applications, vol. 51, no. 3, pp. 2097-2104, May-June 2015.

[19] R. Mikail, I. Husain, Y. Sozer, M. S. Islam and T. Sebastian, "Torque-Ripple Minimization of Switched Reluctance Machines Through Current Profiling," in IEEE Transactions on Industry Applications, vol. 49, no. 3, pp. 1258-1267, May-June 2013.